

Provided for non-commercial research and education use.
Not for reproduction, distribution or commercial use.



(This is a sample cover image for this issue. The actual cover is not yet available at this time.)

This article appeared in a journal published by Elsevier. The attached copy is furnished to the author for internal non-commercial research and education use, including for instruction at the authors institution and sharing with colleagues.

Other uses, including reproduction and distribution, or selling or licensing copies, or posting to personal, institutional or third party websites are prohibited.

In most cases authors are permitted to post their version of the article (e.g. in Word or Tex form) to their personal website or institutional repository. Authors requiring further information regarding Elsevier's archiving and manuscript policies are encouraged to visit:

<http://www.elsevier.com/copyright>



Contents lists available at SciVerse ScienceDirect

Hearing Research

journal homepage: www.elsevier.com/locate/heares

Research paper

Parvalbumin immunoreactivity in the auditory cortex of a mouse model of presbycusis

H.N. Martin del Campo, K.R. Measor, K.A. Razak*

Department of Psychology and Graduate Neuroscience Program, University of California, 900 University Avenue, Riverside, CA 92521, United States

ARTICLE INFO

Article history:

Received 4 July 2012

Received in revised form

30 August 2012

Accepted 31 August 2012

Available online 23 September 2012

ABSTRACT

Age-related hearing loss (presbycusis) affects ~35% of humans older than sixty-five years. Symptoms of presbycusis include impaired discrimination of sounds with fast temporal features, such as those present in speech. Such symptoms likely arise because of central auditory system plasticity, but the underlying components are incompletely characterized. The rapid spiking inhibitory interneurons that co-express the calcium binding protein Parvalbumin (PV) are involved in shaping neural responses to fast spectrotemporal modulations. Here, we examined cortical PV expression in the C57bl/6 (C57) mouse, a strain commonly studied as a presbycusis model. We examined if PV expression showed auditory cortical field- and layer-specific susceptibilities with age. The percentage of PV-expressing cells relative to Nissl-stained cells was counted in the anterior auditory field (AAF) and primary auditory cortex (A1) in three age groups: young (1–2 months), middle-aged (6–8 months) and old (14–20 months). There were significant declines in the percentage of cells expressing PV at a detectable level in layers I–IV of both A1 and AAF in the old mice compared to young mice. In layers V–VI, there was an increase in the percentage of PV-expressing cells in the AAF of the old group. There were no changes in percentage of PV-expressing cells in layers V–VI of A1. These data suggest cortical layer(s)- and field-specific susceptibility of PV+ cells with presbycusis. The results are consistent with the hypothesis that a decline in inhibitory neurotransmission, particularly in the superficial cortical layers, occurs with presbycusis.

© 2012 Elsevier B.V. All rights reserved.

1. Introduction

Presbycusis affects ~35% of humans older than sixty-five and ~45% of humans older than seventy-five years (Gates and Mills, 2005). It is the most prevalent form of hearing impairment and contributes to speech processing deficits, social isolation, depression and may contribute to cognitive impairment in the aged (Weinstein et al., 1982; Frisina and Frisina, 1997; Gates and Mills, 2005; Gates, 2009). Both peripheral and central changes can be involved in presbycusis. Behavioral and physiological studies in humans and rodent models have established that changes in the central auditory system at least partially involve altered temporal processing, which in turn may arise because of altered inhibitory and excitatory properties of neurons (Willott et al., 1993; Walton

et al., 1998; Suta et al., 2011; reviewed in Caspary et al., 2008 and Syka, 2010).

One critical component of inhibitory circuitry involved in sensory processing is the Parvalbumin-expressing (PV+) GABAergic interneuron (Sohal et al., 2009). Parvalbumin expression can decrease, increase, or show no changes with age in a species- and/or area-specific manner (hippocampus, septum, and neocortex of rats: Miettinen et al., 1993; de Villers-Sidani et al., 2010, medial septum-diagonal band of Broca of rats: Krzywkowski et al., 1995; cerebral cortex of humans: Bu et al., 2003; cochlear nucleus of mice: Idrizbegovic et al., 2004; inferior colliculus, medial geniculate body, and auditory cortex of rats: Ouda et al., 2008). The focus on PV+ interneurons in the auditory cortex stems partly because of the association of these neurons with fast temporal processing (Atencio and Schreiner, 2008). Rapid spiking interneurons (presumed PV+) are involved in shaping the inhibitory component of frequency tuning curves in A1 (Wu et al., 2008). The spectrotemporal properties of inhibitory and excitatory components of the frequency tuning curve shape response selectivity for fast spectrotemporal modulations such as those present in frequency modulated (FM) sweeps (Zhang et al., 2003; Razak and Fuzessery, 2006, 2009; Razak, 2012). Frequency modulated sweeps are important for

Abbreviations: AAF, anterior auditory field; A1, primary auditory cortex; AII, secondary auditory cortex; ABR, auditory brainstem recordings; CF, characteristic frequency; FM, frequency modulated; PV+, Parvalbumin immunoreactivity; Y, young mice (1–2 months); M, middle-aged mice (ages 6–8 months); O, old mice (14–20 months).

* Corresponding author. Tel.: +1 951 827 5060.

E-mail address: khaleel@ucr.edu (K.A. Razak).

human speech recognition (Zeng et al., 2005). Physiological and behavioral studies show sensitivity to FM sweeps in rodents (Wetzel et al., 1998; Zhang et al., 2003). The auditory cortex is necessary for behavioral FM sweep discrimination in rodents (Ohl et al., 1993). Mendelson and Ricketts (2001) showed that rat auditory cortical neurons become less selective for fast FM sweeps with age. No changes were seen in the midbrain or thalamus (Lee et al., 2002 and Mendelson and Lui, 2004) suggesting cortex-specific changes in selectivity to fast sweeps. Changes in cortical FM sweep processing may arise because of a decline in PV expression resulting in impaired speech processing. Therefore, it is important to further study presbycusis-related changes in PV+ cells in the auditory cortex.

The auditory cortex contains multiple fields delineated by differences in inputs/outputs, cytoarchitecture, and response selectivity. Differences in response selectivity may in part arise due to differences in inhibitory circuitry across fields. For example, cat A1 and secondary (AII) auditory cortex express different anatomical patterns of PV+ neuron connectivity and these differences may relate to spectral integration properties (Yuan et al., 2011). However, only A1 has been examined in terms of PV expression with aging and hearing loss. There is a decline in PV+ neurons in A1 in a presbycusis rat model, but not in a strain which ages without considerable hearing loss (Ouda et al., 2008). It remains unclear if PV+ cells in different auditory fields are differentially susceptible to presbycusis. There is an age-related increase in PV+ cells in the cochlear nucleus (Idrizbegovic et al., 2004) of a mouse model of presbycusis (the C57bl/6 strain), but if PV expression changes in aging auditory cortex of this strain is not known. The first goal of this study was, therefore, to compare PV expression in A1 and AAF in the C57bl/6 strain mouse.

Auditory response selectivity also changes with cortical depth (Atencio et al., 2009; Trujillo et al., 2011). This may also in part reflect differences in inhibitory circuitry across depth. For example, rabbit infragranular cortical layers show a higher percentage of PV+ cells compared to granular and supragranular layers (McMullen et al., 1994). Hughes et al. (2010) showed that differences in responses to broadband noise between young and old rat A1 neurons was layer-specific in a direction suggestive of greater loss of inhibition in superficial than deeper cortical layers. These data suggest layer-specific susceptibilities of inhibitory neurotransmission with age. The second goal of this study was, therefore, to compare PV expression in layers I–IV and layers V–VI in A1 and AAF.

2. Methods

2.1. Experimental groups

The Institutional Animal Care and Use Committee at the University of California, Riverside approved all procedures. C57 mice were obtained from an in-house breeding colony that originated from breeding pairs purchased from Jackson Laboratory (Bar Harbor, ME). Mice were housed with 2–4 littermates under a 12:12 h light–dark cycle and fed *ad libitum*. All mice were housed in the same vivarium room under similar conditions. The age groups were young ('Y', 1–2 months old), middle-aged ('M', 6–8 months old), and old ('O', 14–20 months old). Twenty-one mice of either sex were used for this study (7 mice per age group).

2.2. Overview

Auditory brainstem recordings (ABR) were conducted to confirm hearing loss in a subset of mice (4 Y, 5 M and 5 O mice) used for PV staining. Multi-unit mapping of the auditory cortex was

conducted in an additional 4 young mice to electrophysiologically identify the border between AAF and A1. Electrophysiological mapping served to provide landmarks to demarcate A1 and AAF. These four mice were not used for PV staining.

2.3. Acoustic stimulation

For both ABR and electrophysiology, acoustic stimulation and data acquisition were driven by custom-written software ('Batlab' developed by Dr. Don Gans, Kent State University, Kent, OH) and a Microstar digital signal processing board. Programmable attenuators (PA5; Tucker-Davis Technologies, Gainesville, FL) allowed control of sound intensities before amplification by an integrated amplifier (Yamaha AX430). Sounds were delivered through a free-field speaker (LCY-K100 ribbon tweeters; Madisound, WI) located 6 inches and 45° from the left ear, contralateral to physiological recordings.

2.4. Surgical procedures

Mice were anesthetized with an i.p. injection of ketamine (150 mg/kg) and xylazine (10 mg/kg) mixture and maintained throughout the experiment via isoflurane inhalation (0.2–0.5% in air). Anesthetic state was monitored throughout the experiment using the toe-pinch reflex test, and isoflurane concentration was adjusted as needed. Once an areflexic state of anesthesia was reached, ABR was determined (see below). For *in vivo* electrophysiology, a scalp incision was made along the midline and the right temporalis muscle was reflected. The skull was scraped clean, and then a craniotomy was performed using a dental drill. The auditory cortex was exposed based on skull and vascular landmarks (Willott et al., 1993). Silicon oil was applied in the exposure to prevent desiccation.

2.5. Auditory brainstem response (ABR)

Experiments were conducted in a heated (80 °F), sound-attenuated chamber lined with anechoic foam (Gretch-Ken Industries, Lakeview, OR). ABRs were measured according to Zheng et al. (1999). Subdermal electrodes were placed in the vertex (active electrode), ventrolateral to the ipsilateral ear (reference electrode) and tail (ground electrode). ABRs were band-pass filtered (0.1–3 kHz) and amplified using a Grass amplifier and displayed/stored on a PC. ABR data from the first 7.5 ms after sound presentation were analyzed. Pure tones (6–40 kHz, 5 ms duration, 0.5 ms rise/fall time, 10 Hz repetition rate, 256 repetitions) were used as ABR stimulus. From 10 to 40 kHz, tone frequencies were varied in 5 kHz steps to measure ABRs. The sound intensity was adjusted between 15 and 100 dB in 5 dB steps (2 dB steps near threshold) to measure thresholds (defined as the lowest intensity producing at least three distinct ABR peaks within 7.5 ms) at each frequency.

2.6. Determination of AAF and A1

As one of the aims was to compare PV expression between AAF and A1, the cortical locations of these two fields had to be determined. The published mouse atlas (Franklin and Paxinos, 2008) distinguishes between primary auditory cortex and secondary auditory cortex but not between AAF and A1. Since it is not possible to distinguish AAF from A1 based on cytoarchitecture, *in vivo* electrophysiology was used to map tonotopy based on the characteristic frequency (CF). The CF increases in a caudal to rostral direction in A1. When CFs reach ~30–40 kHz, they stabilize and then begin to decrease at more rostral recording sites (Willott et al., 1993; Trujillo et al., 2011). This area of CF reversal constitutes

a transition zone between A1 and AAF and contains the boundary between these fields. This transition zone can extend $\sim 150 \mu\text{m}$ and marks a region of uncertainty in terms of where the high-frequency boundary between the two fields is present.

The rostral and caudal edges of AAF were identified based on a single line of electrode placement extending caudal to rostral from A1 to AAF (e.g., Fig. 1). This was accomplished in four 'Y' mice. A two-dimensional tonotopic map is not necessary for the purposes of this study because the CFs change mostly in a caudal to rostral direction in A1/AAF (Trujillo et al., 2011). Additional properties such as first spike latency were also used to mark the transition zone because on average AAF neurons respond earlier than A1 neurons (Linden et al., 2003). The region of CF reversal was identified and marked with a dye as the transition zone. The rostral edge of AAF was dye-marked at the location in AAF beyond which auditory responses could not be elicited with tones and noise. Following brain extraction, sections were cut at $35 \mu\text{m}$. Four sections (total of $140 \mu\text{m}$) around the caudal dye injection site were excluded from data analysis as they fall in the uncertain transition zone. Every fourth section rostral to the transition zone up to the rostral injection site was included as AAF (2–7 sections, Bregma -2.18 to -2.46). Every fourth section caudal to the transition zone up to Bregma -3.40 was included as A1 (3–7 sections, Bregma -2.70 to -3.40). Comparison of our analysis with the published mouse atlas (Franklin and Paxinos, 2008) shows that all sections included in our study lie within what the atlas identifies as primary auditory cortex (Bregma -2.18 to -3.64). The rostrocaudal extent of A1–AAF identified here was similar to that found with more extensive electrophysiological mappings done in young C57 auditory cortex (Trujillo et al., 2011). The dye injections provided hippocampal and Bregma-based landmarks that were then used to identify AAF and A1 in all mice. The assumption that the landmarks/location of AAF/A1 were consistent across the age-groups was made and none of the middle-aged and old mice were mapped. This assumption is justified by the observation that the area of auditory cortex in C57 mice does not change with age (Willott et al., 1993).

2.7. Electrophysiology details

For electrophysiological mapping, mice were placed in a stereotaxic apparatus (model 930; Kopf, Tujunga, CA) and secured in a mouse bite bar adapter (model 923B; Kopf). Multiunit recordings were obtained at cortical depths between 250 and $450 \mu\text{m}$ with glass electrodes filled with 1 M NaCl (impedance 2–10 M Ω). Electrodes were driven orthogonally into the cortex (with a Kopf direct drive 2660 micropositioner). To determine characteristic frequency (CF), pure tones with frequencies between 6 and 40 kHz (resolution 1 kHz, duration between 5 and 10 ms, including 1 ms rise/fall time) and attenuation between 10 and

80 dB were tested. The CF was defined as the frequency at which spikes were generated for at least five successive stimulus presentations at the lowest intensity (minimum threshold). After the low- and high-frequency edge at a given intensity was determined, intensity was decreased in 5-dB steps and the procedure repeated until threshold and CF were determined.

2.8. Dye injection details

Dyes were injected to mark the rostral and caudal borders of AAF. Tips of glass electrodes ($\sim 10 \mu\text{m}$ diameter) were capillary-filled with 20 mg/mL dextran tetramethyl rhodamine (Invitrogen, Carlsbad, CA), diluted with 0.9% normal saline and back filled with 1 M NaCl. The dye was injected using a Midgard precision current source (Stoelting, Wood Dale, IL) with 7 s on–7 s off current stimulus of $+4 \mu\text{A}$. The duration of injection was 5 min at a depth of $\sim 350 \mu\text{m}$. Following histological processing (details below), dye injection sites were viewed with a Nikon Eclipse 80i Microscope with epifluorescent light filters. Images were taken with a Black and White Nikon Digital Sight Camera.

2.9. Immunohistochemistry

Following a lethal injection of sodium pentobarbital (125 mg/kg), mice were transcardially perfused using a peristaltic pump (Fisher Scientific) with 0.1M PBS followed by 4% paraformaldehyde (0.1M PB, pH 7.4). The brains were immediately removed, post-fixed in 4% paraformaldehyde and cryoprotected in 30% sucrose until sinking. Brains were coronally sectioned at $35 \mu\text{m}$ on a cryostat. Immunohistochemistry was carried out with free-floating sections at room temperature with agitation unless otherwise indicated. Sections were pretreated in 0.5% H_2O_2 (in 0.1M PBS, pH 7.4, 30 min) to reduce endogenous peroxidase activity, then rinsed with 0.1% tween-20 detergent (in 0.1M PBS, 3×10 min.), and blocked with 6.7% goat normal serum (s-1000, Vector) (in 0.1M PBS, 2–3 h). Sections were incubated at 4°C in a solution containing rabbit anti-PV (1:5000, PV-25, Swant, Bellinzona, Switzerland), 2% goat normal serum, 0.3% triton X-100 (in 0.1M PBS, 14–19 h). Sections were rinsed in 0.1% tween-20 detergent (in 0.1M PBS, 3×10 min), followed by an incubation in a solution containing Peroxidase-conjugated AffiniPure Goat Anti-Rabbit IgG (H + L) (1:500, Jackson, West Grove, PA), 2% goat normal serum, 0.3% triton X-100 (in 0.1M PBS, 2–3 h). Sections were rinsed (in 0.1M PBS, 3×10 min). Staining was visualized without agitation by first pre-incubating the sections in 3,3'-diaminobenzidine (DAB) (sk-4100, Vector, Burlingame, CA) solution, followed by incubation with H_2O_2 and DAB. Sections were rinsed in dH_2O (2×10 min) transferred to 0.1M PBS, mounted on gelatin-coated slides, air dried, and cover-slipped using DPX mounting medium (Electron Microscopy Sciences).

2.10. Image analysis, counting, and data representation

Nissl- and PV-stained cells were counted only from the left hemisphere of each cortex. Nissl-stained sections were used to identify auditory cortex in the mediolateral axis of each coronal section. Auditory cortex was identified by an increase in cortical thickness, changes in cell density relative to adjacent cortical fields and position relative to the hippocampus (Fig. 2A, left) (Caviness, 1975; Willard and Ryugo, 1983; Wree et al., 1983). The location of auditory cortex was determined on PV+ sections by identifying similar distances from hippocampal landmarks on the PV+ section and adjacent Nissl-stained section (Fig. 2B, left).

NIS Elements advanced research software was used to capture $400 \mu\text{m}$ wide images of the auditory cortex in Nissl- and PV-stained sections (height from white matter to pia). The auditory cortex was

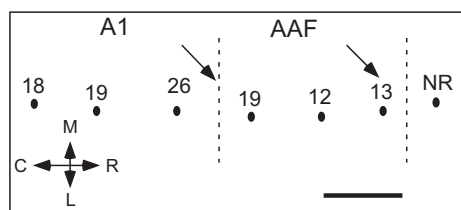


Fig. 1. Electrophysiology and dye injection were used to identify and mark the boundary between A1 and AAF. The figure shows an example sequence of recording sites (filled circles) from a young mouse. The numbers indicate the CF (in kHz) at each recording site. The dashed lines represent the approximate rostral and caudal borders of AAF. The arrows represent the locations of dye injection. Scale bar: $200 \mu\text{m}$. C-caudal; R-rostral; M-medial; L-lateral.

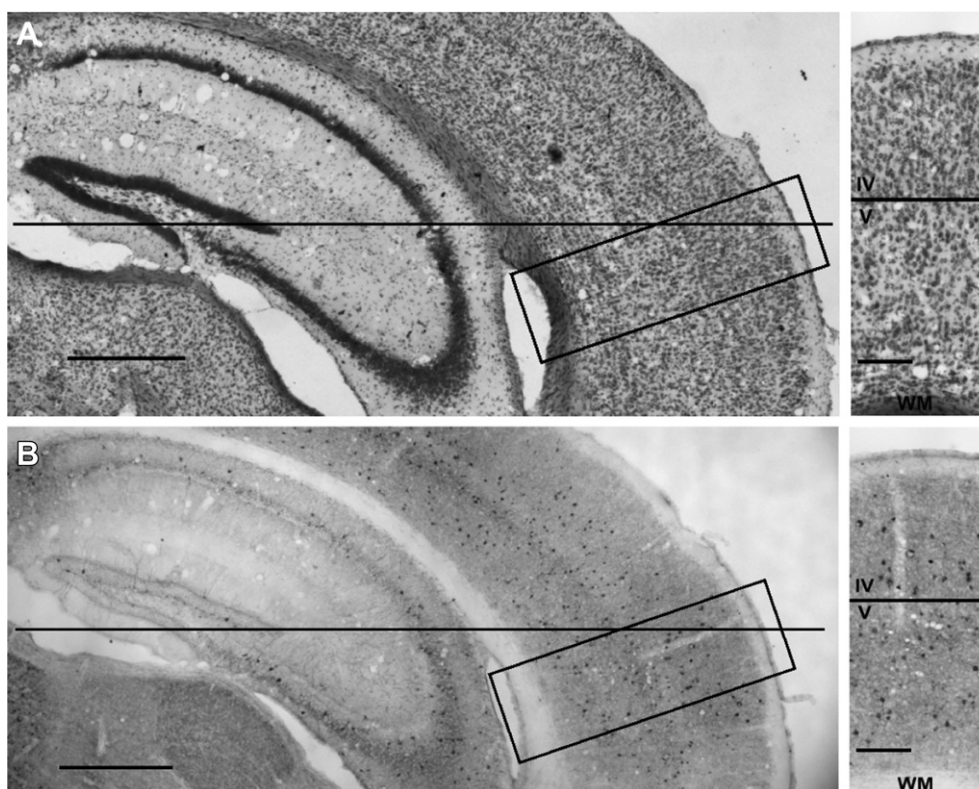


Fig. 2. Identifying auditory cortex and PV+ cells. (A) Left: Nissl-stained coronal section through the AAF. The long horizontal line extends from the hippocampus to the center of the auditory cortex. The rectangle marks the region of auditory cortex sampled for counting. Scale bar: 500 μ m. Right: Nissl-stained section with a horizontal line separating layers IV and V. Placement of line was determined by the changes in laminar distribution of cells between layer IV and V. Scale bar: 200 μ m. (B) Left: Coronal section stained for PV located adjacent to the Nissl stained section in (A). Scale bar: 500 μ m. Right: The horizontal line that separates layers IV/V was drawn at the same distance from pia as the line in the Nissl-stained section (A, right). Scale bar: 200 μ m. Scale bar: 20 μ m. WM: white matter.

divided into layers I–IV and layers V–VI based on the laminar distribution of cells (Fig. 2A, right). Layer IV contains small, densely concentrated cells and layer V contains large, sparsely spaced pyramidal cells (Anderson et al., 2009). The heights of layers I–IV and layers V–VI on each Nissl-stained section were represented as a percentage of total section height (from white matter to pia). These laminar percentages of total height from Nissl-stained sections were used to mark the layer IV/V boundary on adjacent PV+ sections (Fig. 2B, right). Consistent with findings by Anderson et al. (2009), layer IV ended at \sim 50% of total section height for all mice used in this study. Prior to counting, images were adjusted for brightness and contrast using NIS Elements advanced research software. Nissl-stained cells were counted in one of the eight randomly selected 50 μ m wide rectangles within the 400 μ m image of Nissl-stained sections. This count was multiplied by a factor of 8. PV+ cells were counted across the entire 400 μ m wide image of PV stained sections. Only those PV+ cells that had a completely stained soma were included in the counts (e.g., Fig. 2C). Counting bias was avoided by only counting cells that either had their soma contained completely within the image or that fell on the left border of the image. Those cells that fell on the right border of the image were excluded from counting (Gundersen et al., 1988). Data are represented in terms of cell counts or as percentage of PV+ cells relative to Nissl-stained cells. The percentage of PV+ cells relative to Nissl-stained cells will not be affected by possible age-related tissue shrinkage if both PV-stained and Nissl-stained sections shrink by the same amount. Within each age group, the cortical height (from pia to white matter) at the center of the auditory cortex was not different between sections stained for PV compared to the sections stained for Nissl (young cortical height: PV-stained sections:

0.89 ± 0.03 mm, Nissl-stained sections: 0.85 ± 0.06 mm, *t*-test, $p > 0.05$; middle-age cortical height: PV-stained sections: 0.70 ± 0.01 mm, Nissl-stained sections: 0.78 ± 0.02 mm, *t*-test, $p > 0.05$; old cortical height: PV-stained sections: 0.79 ± 0.01 mm, Nissl-stained sections: 0.77 ± 0.02 mm, *t*-test, $p > 0.05$). One-way ANOVA with post-hoc pair-wise comparisons and *t*-tests were used for analysis of histology data. Two-way ANOVA with post-hoc pair-wise comparisons were used for analysis of ABR data. Significance was taken at $p < 0.05$. Table 1 shows the number of sections used for PV immunostaining in each mouse.

3. Results

3.1. ABRs confirm presbycusis

The age-related hearing loss reported in the C57 strain (Henry and Chole, 1980; Hunter and Willott, 1987) was confirmed in a subset of mice used in this study (Fig. 3). The hearing thresholds were significantly different across all three groups (two-way ANOVA, Tukey post hoc pairwise comparison, $p = 0.03$ between 'Y' and 'M', $p < 0.001$ between 'Y' and 'O' and between 'M' and 'O').

3.2. Percentage of PV+ cells in layers I–IV of auditory cortex is reduced in old mice

The number of Nissl-stained cells, PV+ cells and the percentage of PV+ cells (relative to Nissl-stained cells in adjacent sections) in layers I–IV and layers V–VI of the auditory cortex consisting of both A1 and AAF were compared across the three age groups. Fig. 4 shows representative photomicrographs of PV+ cells from each of

Table 1

Each cell shows the number of sections stained for PV expression in each animal. AAF-anterior auditory field; A1-primary auditory cortex.

| | All sections | AAF | A1 |
|--------------------|--------------|-----|----|
| Young | | | |
| MAC376 | 10 | 5 | 5 |
| MAC370 | 10 | 4 | 6 |
| MAC378 | 7 | 4 | 3 |
| MAC375 | 11 | 6 | 5 |
| MAC367 | 9 | 2 | 7 |
| MAC469 | 10 | 6 | 4 |
| MAC468 | 9 | 3 | 6 |
| Middle-aged | | | |
| MAC359 | 9 | 4 | 5 |
| MAC356 | 9 | 4 | 5 |
| MAC354 | 10 | 5 | 5 |
| MAC377 | 10 | 5 | 5 |
| MAC353 | 7 | 4 | 3 |
| MAC433 | 11 | 5 | 6 |
| MAC585 | 12 | 5 | 7 |
| Old | | | |
| MAC361 | 10 | 4 | 6 |
| MAC303(d) | 11 | 6 | 5 |
| MAC319 | 11 | 7 | 4 |
| MAC332 | 12 | 5 | 7 |
| MAC333 | 11 | 5 | 6 |
| MAC305(f) | 11 | 6 | 5 |
| MAC402 | 10 | 4 | 6 |

the three age groups. A decline in the number of PV+ cells in the 'O' mice compared to the 'Y' mice can be seen in these representative examples.

In layers I–IV, there was no change in the number of Nissl-stained cells across the three age groups (Fig. 5A, One-way ANOVA, $p = 0.108$). In layers V–VI, there was a reduction in the number of Nissl-stained cells in the 'O' mice (Fig. 5A, one-way ANOVA, Dunn's post hoc pairwise comparison, $p < 0.05$) compared to both the 'Y' and 'M' mice. The absolute number of PV+ cells declined in the 'O' compared to 'Y' mice in layers I–IV (Fig. 5B, one-way ANOVA, Tukey post hoc pairwise comparison, $p < 0.001$). There was no change in absolute number of PV+ cells in layers V–VI across the three age groups (Fig. 5B). There was a significant decline in the percentage of

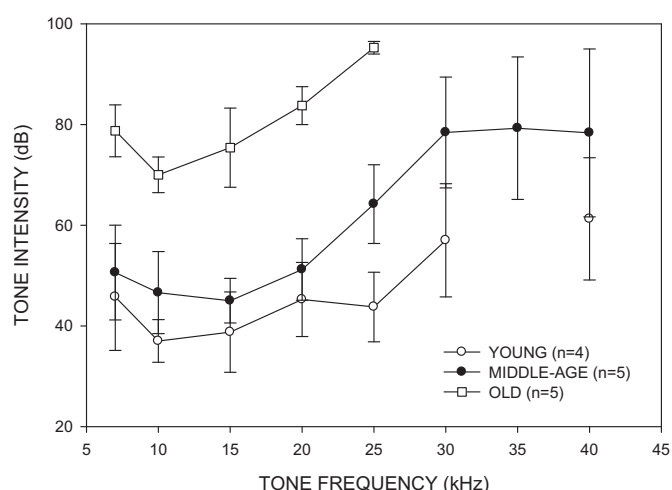


Fig. 3. Comparison of ABRs across young (solid circle), middle aged (open circle), and old animals (open square). Error bars are for SEM. There is a significant difference in hearing threshold across all three age groups, with both middle-aged and old mice showing hearing loss compared to young mice. There are no data for frequencies >25 kHz for the old mice because there was no response at any of the intensities tested for these frequencies. There are no data for 35 kHz in the young group because this frequency was not tested in the young mice.

PV+ cells in layers I–IV in the 'O' mice (Fig. 5C, one-way ANOVA, Tukey post hoc pairwise comparison, $p = 0.001$) compared to the 'Y' mice. Thus, the reduction in PV+ cells in layers I–IV of the auditory cortex appears to be specific to this cell class and not due to general neuronal death. There was no change in the percentage of PV+ in layers V–VI (Fig. 5C). These data suggest layer-specific susceptibility of PV+ cells in the auditory cortex of aging C57 mice.

3.3. Field- and layer-specific susceptibility of PV+ cells

The number of Nissl-stained cells, PV+ cells, and the percentage of PV+ cells in layers I–IV and layers V–VI were compared separately for AAF and A1 across the three age groups.

3.3.1. Anterior auditory field

There was no change in Nissl-stained cell count in layers I–IV of AAF (Fig. 5D). In layers V–VI, however, the number of Nissl-stained cells decreased in both the 'M' and 'O' mice compared to 'Y' (Fig. 5D, one-way ANOVA, Tukey's post hoc pairwise comparison, $p < 0.001$). The absolute number of PV+ cells decreased in layers I–IV in both 'M' (Fig. 5E, one-way ANOVA, Tukey post-hoc pairwise comparison, $p = 0.05$) and 'O' mice (Fig. 5E, one-way ANOVA, Tukey post hoc pairwise comparison, $p = 0.025$) compared to 'Y' mice. The percentage of PV+ cells in layers I–IV of AAF was significantly reduced in the 'O' compared to the 'Y' mice (Fig. 5F, one-way ANOVA, Tukey post-hoc pairwise comparison, $p = 0.035$). A non-significant decline in the percentage of PV+ neurons in layers I–IV in 'M' mice was present (Fig. 5F, one-way ANOVA, Tukey post-hoc pairwise comparison, $p = 0.069$). Thus, there is a significant decline in the percentage of PV+ cells in layers I–IV of AAF with age that appears to be specific to this cell class and not due to overall declines in cells number. There was no change in the absolute number of PV+ cells in layers V–VI in AAF (Fig. 5E). However, the 'O' mice showed a higher percentage of PV+ than both 'Y' and 'M' groups (Fig. 5F, one-way ANOVA, $p = 0.037$) in layers V–VI. This increase is notable because absolute number of PV+ cells remained stable with age in layers V–VI while Nissl-stained cells declined in number, suggesting viability of PV+ neurons as other cells die in layers V–VI.

3.3.2. Primary auditory cortex

There was no change in the number of Nissl-stained cells in layers I–IV of A1 (Fig. 5G). Layers V–VI of A1 showed a reduction in Nissl-stained cells in the 'O' compared to the 'Y' and 'M' mice (Fig. 5G, one-way ANOVA, Tukey post hoc pairwise comparison, $p < 0.001$). In layers I–IV, the number of PV+ cells decreased in the 'O' compared to the 'M' (Fig. 5H, one-way ANOVA, Tukey post hoc pairwise comparison, $p = 0.033$) and 'Y' mice (Fig. 5H, one-way ANOVA, Tukey post hoc pairwise comparison, $p = 0.004$). There was no significant change in the number of PV+ cells in layers V–VI (Fig. 5H, one-way ANOVA, $p = 0.145$). As in AAF, the percentage of PV+ cells in A1 layers I–IV for 'O' mice was significantly less than that in 'Y' mice (Fig. 5I, one-way ANOVA, Tukey post-hoc pairwise comparison, $p = 0.027$). However, unlike AAF, there was no change in percentage of PV+ cells in layers V–VI in A1 (Fig. 5I).

3.4. Comparison of percentage of PV+ cells between layers and fields within age groups

We compared the percentage of PV+ cells between layers within each age group. When sections from A1 and AAF were combined, there was a significantly higher percentage of PV+ cells in layers V–VI compared to layers I–IV within each group (Table 2, left). When each field was considered individually, layer-specific differences in PV cells were age-dependent in AAF, but not in A1.

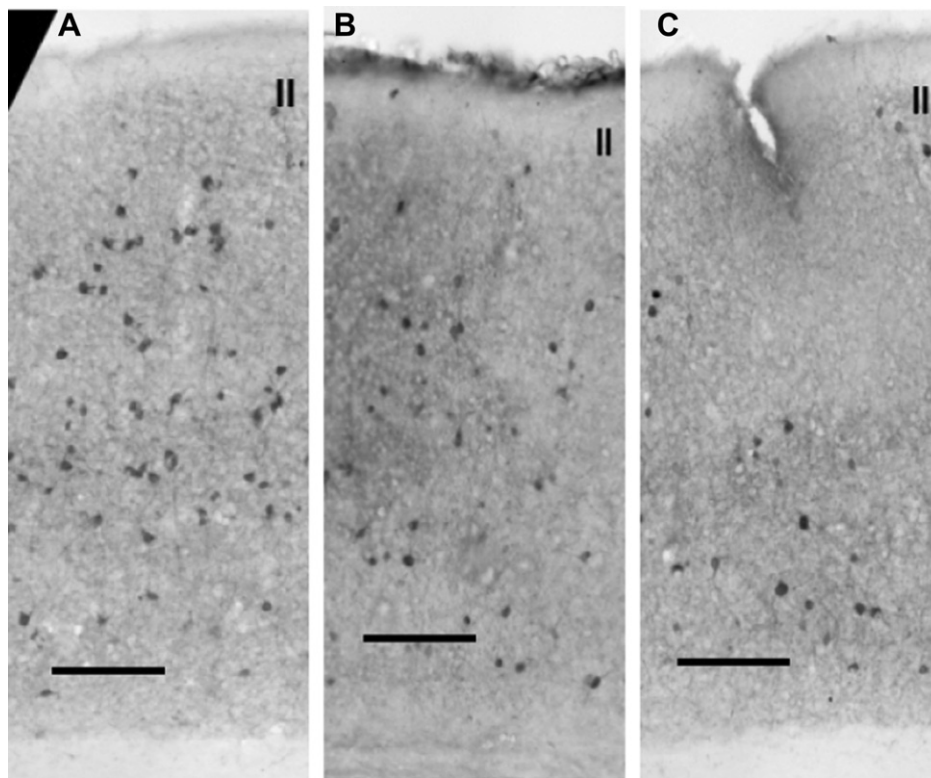


Fig. 4. Decrease in PV+ cells in auditory cortex. Representative photomicrographs of PV+ cell staining in (A) young, (B) middle-aged, and (C) old animals. Roman numeral represents beginning of cortical layer II. A decrease in the number of PV+ cells with age is apparent. Scale bar: 150 μ m.

Specifically, in AAF, the 'Y' group showed no difference in the percentage of PV+ cells between layers I–IV and layers V–VI. In the 'M' and 'O' mice, however, the deeper layers showed a higher percentage of PV+ cells. In A1, there was a higher percentage of PV+ cells in layers V–VI compared to layers I–IV across all age groups (Table 2, right). We also compared the percentage of PV+ cells between fields within each age group (Table 3). There were no field-specific differences in the percentage of PV+ cells within an age group/layer association. In other words, the percentage of PV+ cells in layers I–IV was similar between A1 and AAF in each age group. This was also true for layers V–VI.

4. Discussion

The main finding of this study is a decline in the percentage of cells expressing PV at a detectable level in the auditory cortex of aging C57 mice. The decline was found in layers I–IV but not in the deeper layers V–VI, indicating layer-specific susceptibility of PV expression. Both A1 and AAF showed similar declines in the percentage of PV-expressing cells in layers I–IV. In layers I–IV of either field, there was no change in the number of Nissl-stained cells suggesting that the observed result may be due to reduced PV expression rather than neuronal death. In layers V–VI, there were field-specific differences in percentage of cells expressing PV. AAF in the old mice showed an increase while there was no difference in A1. In AAF, the observed increase in percentage of PV+ cells was due to decreased number of Nissl-stained cells, and not due to an increase in the absolute number of PV+ cells. This indicates PV expression remains viable in deeper layers as other cells die. Taken together, these data indicate complex field- and layer-specific changes in PV expression in a mouse model of presbycusis. These data support the notion of a presbycusis-associated decrease in inhibitory neurotransmission that affects superficial

layers to a greater extent than deep layers in the auditory cortex (Ling et al., 2005; Hughes et al., 2010).

Our data does not allow disambiguation of age *versus* hearing loss as the factor underlying reduction in PV expression. Data in the Fischer 344 rat A1, a strain susceptible to hearing loss, show a decline in cortical PV expression with age (Ouda et al., 2008). There was no age-related decline in the Long-Evans rat strain in which accelerated hearing loss is not seen (Ouda et al., 2008). To the extent that the genetics of different strains was not a factor, this indicates hearing loss dependent changes in activity levels, and not age, was the driving factor in reduced PV expression. The trend toward a decline in the number of PV expressing cells even in the middle-age C57 mice is consistent with an experience-dependent (hearing loss) change. In Fischer 344 rats, behavioral training can prevent cortical PV expression decline, further supporting the notion that PV expression is experience-dependent (de Villers-Sidani et al., 2010). Experience-dependent decline in PV expression was also reported in the enucleated hamster and the blind Crx^{-/-} mouse visual cortex (Desgent et al., 2010; Goldshmit et al., 2010). Bu et al. (2003) reported that there was no age-related decline in PV expression in human A1, but it was not clear if hearing loss was involved.

Most cortical PV+ interneurons are of the rapid spiking GABAergic phenotype and are involved in shaping the inhibitory component of auditory receptive fields (Wu et al., 2008) and processing sounds with rapid temporal changes (Atencio and Schreiner, 2008). The role of PV+ cells in temporal processing is also indicated by their contributions to gamma-band oscillation and sensory processing (Bartos et al., 2007; Buzsaki and Draguhn, 2004; Sohal et al., 2009). There is an age-related decline in response selectivity to rapid temporal cues specific to the auditory cortex in rats (Mendelson and Ricketts, 2001). A similar decline is also found in the C57 mouse cortex (Trujillo and Razak, unpublished observations). These findings implicate reduced expression

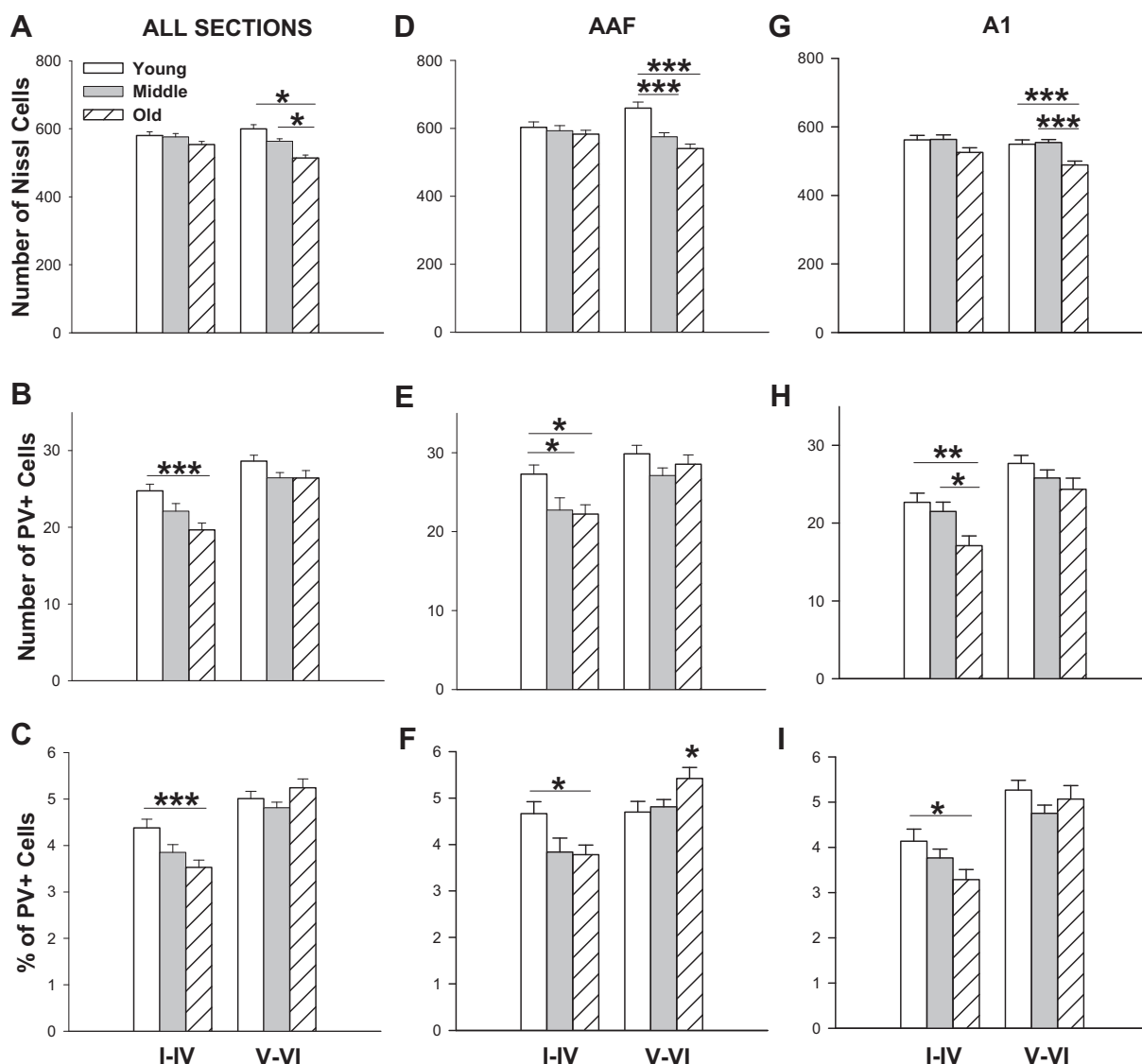


Fig. 5. Decrease in PV+ in layers I–IV in AAF and A1. Data were plotted for all sections (left column), AAF (middle column), and A1 (right column). (A, D, G) Mean number of Nissl-stained cells within 400 μm width cortical columns. The height of each column extended from the pia to white matter. (B, E, H) Mean number of PV+ cells within 400 μm width cortical columns. The height of each column extended from the pia to white matter. (C, F, I) Percentage of PV+ cells relative to Nissl-stained cells. On each graph, the left group of bars are layers I–IV, and the right group of bars are layers V–VI. *: $p \leq 0.050$. **: $p \leq 0.010$. ***: $p \leq 0.001$. Error bars are for SEM. Horizontal lines show pairwise comparison.

of PV as a possible source of presbycusis-related decline in cortical spectrotemporal analysis involved in processing of complex stimuli (de Villers-Sidani et al., 2010).

4.1. Expression of PV+ cells in the young auditory cortex: comparison with previous studies

There was no difference in percentage of cells expressing PV between A1 and AAF within any age group (Table 3). PV+ immunoreactivity in A1 is greater than in secondary auditory cortical areas in mice (Cruikshank et al., 2001), monkeys (Jones, 2003) and humans (Chiry et al., 2003). Both A1 and AAF are considered part of the core auditory cortex in mice, and therefore the lack of difference in PV expression between A1 and AAF is not surprising. Whether differences exist between mouse A1 and AAF in the connections of PV+ neurons as seen between A1 and AII of the cat (Yuan et al., 2011) remains to be investigated.

There are species-specific differences in the overall percentage of PV+ in A1. In the cat, 13% of the cells in A1 are PV+ (Yuan et al.,

2011). This is in contrast to the lower levels found in the rabbit (~7%, McMullen et al., 1994) and C57 mouse (~5%, our data) A1. In addition there are species-specific differences in the laminar distribution of PV+ cells. In the cat A1, layers II/III show more PV+ cells compared to deeper cortical layers (Clemo et al., 2003). In the rabbit A1, deeper layers (IV–VI) have the highest percentages of PV+ (10–11%) with a decline in PV+ superficially (6%, 3% and 5% for layers III, II, I, respectively) (McMullen et al., 1994). Young C57 A1 is similar to the rabbit with a higher percentage of PV+ cells in layers V–VI than layers I–IV. Interestingly, the laminar distribution of the percentage of PV+ cells in AAF is in contrast to both cats and rabbits, with similar levels found in layers I–IV as in layers V–VI.

4.2. Why are PV positive cells in auditory cortex susceptible to presbycusis?

An intriguing question of clinical importance is why the PV-expressing class of interneurons is susceptible to presbycusis-related decline in the auditory cortex. Recent studies have

Table 2
Laminar comparison of percentage of PV+ cells within age groups. Each cell shows the percentage of PV+ cells relative to Nissl-stained cells. *p*-values of *t*-tests are shown for comparison of cortical layers I–IV and V–VI for all sections and separately for A1 and AAF.

| | All sections | | | AAF | | | A1 | | |
|--------|--------------|--------------|----------------|--------------|--------------|----------------|--------------|--------------|----------------|
| | I–IV | V–VI | <i>t</i> -Test | I–IV | V–VI | <i>t</i> -Test | I–IV | V–VI | <i>t</i> -Test |
| Young | 4.4% ± 0.188 | 5.0% ± 0.160 | 0.012 | 4.7% ± 0.253 | 4.7% ± 0.229 | 0.924 | 4.1% ± 0.268 | 5.3% ± 0.216 | 0.002 |
| Middle | 3.8% ± 0.170 | 4.8% ± 0.121 | <0.001 | 3.8% ± 0.301 | 4.8% ± 0.157 | <0.001 | 3.8% ± 0.193 | 4.8% ± 0.182 | <0.001 |
| Old | 3.5% ± 0.154 | 5.2% ± 0.193 | <0.001 | 3.8% ± 0.208 | 5.4% ± 0.236 | <0.001 | 3.3% ± 0.223 | 5.1% ± 0.298 | <0.001 |

suggested PGC1 α , a transcriptional co-activator important in regulation of cellular metabolism is involved in PV expression in the cerebral cortex (Lucas et al., 2010). PGC1 α knock-out mice show reduced expression of PV in GABAergic cells, and this reduction causes reduced inhibitory neurotransmission. PV expression can be increased in cultured neurons by PGC1 α over-expression. It is likely that the observed reduction in PV expression in the aged mouse auditory cortex also results in reduced inhibition. Together with the observed age-related decline in the GABA synthetic enzyme glutamic acid decarboxylase (GAD) in A1 (Ling et al., 2005), the present data support the hypothesis that inhibitory neurotransmission is vulnerable during aging. PV expression appears to be particularly vulnerable to changes in activity levels as observed in the ketamine model of schizophrenia (Behrens et al., 2007) and models of epilepsy (Sloviter, 1991; Best et al., 1993). This vulnerability is mediated largely by activation of pathways related to oxidative stress (Powell et al., 2012). Thus in presbycusis, the reduced level of excitation driven through inputs in the hearing loss range may initially lead to hypoactivation of the PV neurons causing a compensatory decrease in GAD, GABA, PGC1 α and PV. PGC1 α is involved in neuroprotection against oxidative stress leading to vulnerability of PV expressing GABAergic neurons to presbycusis-related build up of stress. Whether a layer- and field-specific decline in PGC1 α occurs upstream of PV expression decline will be investigated in the future.

4.3. Methodological considerations

There were two methodological issues in this study that could have influenced the data. First, both males and females were used. There was a bias, such that most (5 out of 7) young mice studied were males, and most middle-aged (6 out of 7) and old (4 out of 7) mice studied were females. The differences in circulating estrogens may have influenced the data, but the literature suggests a neuroprotective effect (reviewed in Hultcrantz et al., 2006). This suggests that the decline reported in the older group may be an underestimation. The second issue was in relation to correctly identifying sections from A1 and AAF. As mentioned in the Methods, A1 and AAF cannot be demarcated using histology alone. Therefore we used electrophysiological mapping. Even with mapping, there is a relatively broad transition zone within which the boundary is present. We excluded this transition zone because of the ambiguity in whether the sections belong to A1 or AAF. However, this

Table 3
Auditory cortical field comparison of percentage of PV+ cells within age groups. Each data cell in the table shows percentage of PV+ cells in the auditory cortical fields, A1 and AAF. *p*-values for layer-specific comparison of the two fields are shown.

| | Layers I–IV | | | Layers V–VI | | |
|--------|--------------|--------------|----------------|--------------|--------------|----------------|
| | AAF | A1 | <i>t</i> -Test | AAF | A1 | <i>t</i> -Test |
| Young | 4.7% ± 0.253 | 4.1% ± 0.268 | 0.161 | 4.7% ± 0.229 | 5.3% ± 0.216 | 0.078 |
| Middle | 3.8% ± 0.301 | 3.8% ± 0.193 | 0.839 | 4.8% ± 0.157 | 4.8% ± 0.182 | 0.812 |
| Old | 3.8% ± 0.208 | 3.3% ± 0.223 | 0.110 | 5.4% ± 0.236 | 5.1% ± 0.298 | 0.359 |

transition zone is where most high-CF neurons are present. If our contention that PV neurons decline is because of activity-dependent plasticity, then in a high-frequency hearing loss model, the transition zone is where most changes will occur. Once, again the decline shown in the old group may be an underestimate.

Acknowledgments

We thank the members of the Razak lab for reviewing this paper and the Deafness Research Foundation for funding this study.

References

Anderson, L.A., Christianson, G.B., Linden, J.F., 2009. Mouse auditory cortex differs from visual and somatosensory cortices in the laminar distribution of cytochrome oxidase and acetylcholinesterase. *Brain Res.* 1252, 130–142.

Atencio, C.A., Schreiner, C.E., 2008. Spectrotemporal processing differences between auditory cortical fast-spiking and regular-spiking neurons. *J. Neurosci.* 28, 3897–3910.

Atencio, C.A., Sharpee, T.O., Schreiner, C.E., 2009. Hierarchical computation in the canonical auditory cortical circuit. *Proc. Natl. Acad. Sci. U.S.A.* 106, 21894–21899.

Bartos, M., Vida, I., Jonas, P., 2007. Synaptic mechanisms of synchronized gamma oscillations in inhibitory interneuron networks. *Nat. Rev. Neurosci.* 8, 45–56.

Behrens, M.M., Ali, S.S., Dao, D.N., Lucero, J., Shekhtman, G., Quick, K.L., Dugan, L.L., 2007. Ketamine-induced loss of phenotype of fast-spiking interneurons is mediated by NADPH-oxidase. *Science* 318, 1645–1647.

Best, N., Mitchell, J., Baimbridge, K.G., Wheal, H.V., 1993. Changes in parvalbumin-immunoreactive neurons in the rat hippocampus following a kainic acid lesion. *Neurosci. Lett.* 155, 1–6.

Bu, J., Sathyendra, V., Nagykerly, N., Geula, C., 2003. Age-related changes in calbindin-D_{28k}, calretinin, and parvalbumin-immunoreactive neurons in the human cerebral cortex. *Exp. Neurol.* 182, 220–231.

Buzsaki, G., Draguhn, A., 2004. Neuronal oscillations in cortical networks. *Science* 304 (5679), 1926–1929.

Caspary, D.M., Ling, L., Turner, J.G., Hughes, L.F., 2008. Review inhibitory neurotransmission, plasticity and aging in the mammalian central auditory system. *J. Exp. Biol.* 211, 1781–1791.

Caviness, V.S., 1975. Architectonic map of neocortex of the normal mouse. *J. Comp. Neurol.* 164, 247–263.

Chiry, O., Tardif, E., Magistretti, P.J., Clarke, S., 2003. Patterns of calcium-binding proteins support parallel and hierarchical organization of human auditory areas. *Eur. J. Neurosci.* 17, 397–410.

Clemon, H.R., Keniston, L., Meredith, M.A., 2003. Comparison of the distribution of GABA-ergic neurons in cortices representing different sensory modalities. *J. Chem. Neuroanat.* 26, 51–63.

Cruikshank, S.J., Killackey, H.P., Metherate, R., 2001. Parvalbumin and calbindin are differentially distributed within primary and secondary subregions of the mouse auditory forebrain. *Neuroscience* 105, 553–569.

de Villers-Sidani, E., Alzghoul, L., Zhou, X., Simpson, K.L., Lin, R.C., Merzenich, M.M., 2010. Recovery of functional and structural age-related changes in the rat primary auditory cortex with operant training. *Proc. Natl. Acad. Sci. U.S.A.* 107, 13900–13905.

Desgent, S., Boire, D., Ptilo, M., 2010. Altered expression of parvalbumin and calbindin in interneurons within the primary visual cortex of neonatal enucleated hamsters. *Neuroscience* 171, 1326–1340.

Franklin, K.B., Paxinos, G., 2008. *The Mouse Brain in Stereotaxic Coordinates*. Academic Press, San Diego, CA.

Frisina, D.R., Frisina, R.D., 1997. Speech recognition in noise and presbycusis: relations to possible neural mechanisms. *Hear. Res.* 106, 95–104.

Gates, G.A., 2009. Central auditory processing in presbycusis: an epidemiological perspective. In: *Hearing Care for Adults*, pp. 47–52.

Gates, G.A., Mills, J.H., 2005. Presbycusis. *The Lancet* 366, 1111–1120.

Goldshmit, Y., Galley, S., Foo, D., Sernagor, E., Bourne, J.A., 2010. Anatomical changes in the primary visual cortex of the congenitally blind Crx^{-/-} mouse. *Neuroscience* 166, 886–898.

- Gundersen, H.J.G., Bendtsen, T.F., Korbo, L., Marcussen, N., Moller, A., Nielsen, K., Nyengaard, J.R., Pakkenberg, B., Sorensen, F.B., Vesterby, A., West, M.J., 1988. Some new, simple and efficient stereological methods and their use in pathological research and diagnosis. *APMIS* 96, 379–394.
- Henry, K.R., Chole, R.A., 1980. Genotypic differences in behavioral, physiological and anatomical expressions of age-related hearing loss on the laboratory mouse. *Audiology* 19, 369–383.
- Hultcrantz, M., Simonoska, R., Stenberg, A.E., 2006. Estrogen and hearing: a summary of recent investigations. *Acta Otolaryngol.* 126, 10–14.
- Hughes, L.F., Turner, J.G., Parrish, J.L., Caspary, D.M., 2010. Processing of broadband stimuli across A1 layers in young and aged rats. *Hear. Res.* 264, 79–85.
- Hunter, K.P., Willott, J.F., 1987. Aging and the auditory brainstem response in mice with severe or minimal presbycusis. *Hear. Res.* 30, 207–218.
- Idrizbegovic, E., Bogdanovic, N., Willott, J.F., Canlon, B., 2004. Age-related increases in calcium-binding protein immunoreactivity in the cochlear nucleus of hearing impaired C57BL/6J mice. *Neurobiol. Aging* 25, 1085–1093.
- Jones, E.G., 2003. Chemically defined parallel pathways in the monkey auditory system. *Ann. N.Y. Acad. Sci.* 999, 218–233.
- Krzywkowski, P., De Bilbao, F., Senut, M.C., Lamour, Y., 1995. Age-related changes in parvalbumin- and GABA-immunoreactive cells in the rat septum. *Neurobiol. Aging* 16, 29–40.
- Lee, H.J., Wallani, T., Mendelson, J.R., 2002. Temporal processing speed in the inferior colliculus of young and aged rats. *Hear. Res.* 174, 64–74.
- Linden, J.F., Liu, R.C., Sahani, M., Schreiner, C.E., Merzenich, M.M., 2003. Spectrotemporal structure of receptive fields in areas AI and AAF of mouse auditory cortex. *J. Neurophysiol.* 90, 2660–2675.
- Ling, L.L., Hughes, L.F., Caspary, D.M., 2005. Age-related loss of the GABA synthetic enzyme glutamic acid decarboxylase in rat primary auditory cortex. *Neuroscience* 132, 1103–1113.
- Lucas, E.K., Markwardt, S.J., Gupta, S., Meador-Woodruff, J.H., Lin, J.D., Overstreet-Wadiche, L., Cowell, R.M., 2010. Parvalbumin deficiency and GABAergic dysfunction in mice lacking PGC-1alpha. *J. Neurosci.* 30, 7227–7235.
- McMullen, N.T., Smelser, C.B., deVenecia, R.K., 1994. A quantitative analysis of parvalbumin neurons in rabbit auditory neocortex. *J. Comp. Neurol.* 349, 493–511.
- Mendelson, J.R., Lui, B., 2004. The effects of aging in the medial geniculate nucleus: a comparison with the inferior colliculus and auditory cortex. *Hear. Res.* 191, 21–33.
- Mendelson, J.R., Ricketts, C., 2001. Age-related temporal processing speed deterioration in auditory cortex. *Hear. Res.* 158, 84–94.
- Miettinen, R., Sirvio, J., Riekkinen, P., Laakso, M.P., Riekkinen, M., Riekkinen, P., 1993. Neocortical, hippocampal and septal parvalbumin- and somatostatin-containing neurons in young and aged rats: correlation with passive avoidance and water maze performance. *Neuroscience* 52, 367–378.
- Ohl, F.W., Wetzels, W., Wagner, T., Rech, A., Scheich, H., 1993. Bilateral ablation of auditory cortex in Mongolian gerbil affects discrimination of frequency modulated tones but not of pure tones. *Learn. Mem.* 6, 347–362.
- Ouda, L., Druga, R., Syka, J., 2008. Changes in parvalbumin immunoreactivity with aging in the central auditory system of the rat. *Exp. Gerontol.* 43, 782–789.
- Powell, S.B., Sejnowski, T.J., Behrens, M.M., 2012. Behavioral and neurochemical consequences of cortical oxidative stress on parvalbumin-interneurons maturation in rodent models of schizophrenia. *Neuropharmacology* 62, 1322–1331.
- Razak, K.A., 2012. Mechanisms underlying intensity-dependent changes in cortical selectivity for frequency modulated sweeps. *J. Neurophysiol.* 107, 2202–2211.
- Razak, K.A., Fuzessery, Z.M., 2009. GABA shapes selectivity for the rate and direction of frequency-modulated sweeps in the auditory cortex. *J. Neurophysiol.* 102, 1366–1378.
- Razak, K.A., Fuzessery, Z.M., 2006. Neural mechanisms underlying selectivity for the rate and direction of frequency-modulated sweeps in the auditory cortex of the pallid bat. *J. Neurophysiol.* 96, 1303–1319.
- Sloviter, R.S., 1991. Permanently altered hippocampal structure, excitability, and inhibition after experimental status epilepticus in the rat: the "dormant basket cell" hypothesis and its possible relevance to temporal lobe epilepsy. *Hippocampus* 1, 41–66.
- Sohal, V.S., Zhang, F., Yizhar, O., Deisseroth, K., 2009. Parvalbumin neurons and gamma rhythms enhance cortical circuit performance. *Nature* 459, 698–702.
- Suta, D., Rybalko, N., Pelanova, J., Popelar, J., Syka, J., 2011. Age related changes in auditory temporal processing in the rat. *Exp. Gerontol.* 46, 739–746.
- Syka, J., 2010. The Fischer 344 rat as a model of presbycusis. *Hear. Res.* 264, 70–78.
- Trujillo, M., Measor, K., Carrasco, M.M., Razak, K.A., 2011. Selectivity for the rate of frequency-modulated sweeps in the mouse auditory cortex. *J. Neurophysiol.* 106, 2825–2837.
- Walton, J.P., Frisina, R.D., O'Neil, W.E., 1998. Age-related alteration in processing of temporal sound features in the auditory midbrain of the CBA mouse. *J. Neurosci.* 18, 2764–2776.
- Weinstein, B.E., Ventry, I.M., 1982. Hearing impairment and social isolation in the elderly. *J. Speech Hear. Res.* 25, 593–599.
- Wetzels, W., Wagner, T., Ohl, F.W., Scheich, H., 1998. Categorical discrimination of direction in frequency-modulated tones by Mongolian gerbils. *Behav. Brain Res.* 91, 29–39.
- Willard, F.H., Ryugo, D.K., 1983. Anatomy of the central auditory system. In: Willott, J.F. (Ed.), *The Auditory Psychobiology of the Mouse*. Charles C. Thomas, Springfield, IL, pp. 201–304.
- Willott, J.F., Aitkin, L.M., McFadden, S.L., 1993. Plasticity of auditory cortex associated with sensorineural hearing loss in adult C57BL/6J mice. *J. Comp. Neurol.* 329, 402–411.
- Wree, A., Zilles, K., Schleicher, A., 1983. A quantitative approach to cytoarchitectonics VIII. The areal pattern of the cortex of the albino mouse. *Anat. Embryol.* 166, 333–353.
- Wu, G.K., Arbuckle, R., Lui, B., Tao, H.W., Zhang, L.L., 2008. Lateral sharpening of cortical frequency tuning by approximately balanced inhibition. *Neuron* 58, 132–143.
- Yuan, K., Shih, J.Y., Winer, J.A., Schreiner, C.E., 2011. Functional networks of parvalbumin-immunoreactive neurons in cat auditory cortex. *J. Neurosci.* 31, 13333–13342.
- Zeng, F.G., Nie, K., Stickney, G.S., Kong, Y.Y., Vonghoh, M., Bhargava, A., Wei, C., Cao, K., 2005. Speech recognition with amplitude and frequency modulations. *PNAS* 102, 2293–2298.
- Zhang, L.L., Tan, A.Y.Y., Schreiner, C.E., Merzenich, M.M., 2003. Topography and synaptic shaping of direction selectivity in primary auditory cortex. *Nature* 424, 201–205.
- Zheng, Q.Y., Johnson, K.R., Erway, L.C., 1999. Assessment of hearing in 80 inbred strains of mice by ABR threshold analyses. *Hear. Res.* 130, 94–107.